

Effects of nonlinear photoemission on mean transverse energy from metal photocathodes

Christopher J. Knill^{1,*}, Stephen Douyon,¹ Kenji Kawahara², Hisato Yamaguchi,³ Gaoxue Wang,³ Hiroki Ago², Nathan Moody,³ and Siddharth Karkare^{1,†}

¹*Department of Physics, Arizona State University, Tempe, Arizona 85287, USA*

²*Global Innovation Center, Kyushu University, Kasuga, Fukuoka, 816-8580, Japan*

³*Los Alamos National Laboratory, Los Alamos, New Mexico 87545, USA*

 (Received 27 June 2023; accepted 29 August 2023; published 19 September 2023)

Reducing the mean transverse energy (MTE) of electrons emitted from photocathodes will improve the performance of linear accelerator applications like x-ray free electrons lasers (XFELs) and ultrafast electron diffraction (UED) and microscopy (UEM) experiments. Metallic photocathodes are popular for these applications due to their convenience of use. However, they typically have a very low quantum efficiency and require a large laser fluence in order to extract the desired charge density for applications like XFELs and single-shot UED/UEM experiments. Recent theoretical investigations have shown that nonlinear photoemission effects of multiphoton emission and electron heating increase the MTE dramatically at these large laser fluences. In this paper, we report on measurements of nonlinear near-threshold photoemission from a graphene-coated Cu(110) photocathode at laser pulse lengths of 130 fs, 1 ps, and 10 ps. We extrapolate our measured data to find the ideal irradiating photon energy that results in a minimum MTE from such metallic photocathodes for charge densities relevant to photoinjectors and specify quantum efficiency requirements to obtain the thermally limited MTE at these charge densities.

DOI: [10.1103/PhysRevAccelBeams.26.093401](https://doi.org/10.1103/PhysRevAccelBeams.26.093401)

I. INTRODUCTION

The brightness of ultrafast electron pulses generated by photoinjectors is crucial to the performance of linear accelerator applications like x-ray free electron lasers (XFELs) and single-shot ultrafast electron diffraction (UED) and microscopy (UEM) experiments. For XFELs, a brighter electron beam will increase both the x-ray pulse energy and the maximum lasing energies [1]. In addition, a brighter beam will enable the construction of smaller, university-scale XFELs which will significantly increase the accessibility of these experiments to the scientific community [2]. For single-shot UED/UEM experiments, a brighter electron beam will increase the transverse coherence length and thus the spatial-temporal resolution [3]. This will enable the study of larger lattice sizes like

proteins and macromolecular assemblies increasing the scientific capability of UED/UEM experiments.

For the above applications, the maximum beam brightness occurs at the photoemission source, or photocathode, and is given by the following relation:

$$B \propto \frac{E^n}{\text{MTE}}, \quad (1)$$

where E is the accelerating electric field; n is a real number between 1 and 2 which depends on the design of the photoinjector; and MTE is the mean transverse energy of the photocathode [4]. The MTE is also related to the normalized transverse emittance $\varepsilon_{n,x}$ at the photocathode via the following relationship:

$$\varepsilon_{n,x}/\sigma_x = \sqrt{\text{MTE}/m_e c^2}, \quad (2)$$

where σ_x is the rms laser spot size; m_e is the mass of the electron; and c is the speed of light. The MTE is the key figure of merit in determining the brightness of the electron beam and it is equivalent to the temperature of the electrons in vacuum [4]. Hence, understanding and minimizing the MTE are necessary to achieve the brightest possible electron beams for linear accelerator applications.

*To whom all correspondence should be addressed: cknill2@asu.edu

†To whom all correspondence should be addressed: karkare@asu.edu

Published by the American Physical Society under the terms of the Creative Commons Attribution 4.0 International license. Further distribution of this work must maintain attribution to the author(s) and the published article's title, journal citation, and DOI.

Using Spicer's three-step model of photoemission, Dowell and Schmerge demonstrated that for typical metallic photocathodes, the MTE roughly obeys

$$\text{MTE} = \frac{E_{\text{excess}}}{3}, \quad (3)$$

where E_{excess} is the excess energy and is defined as the difference between the photon energy ($\hbar\omega$) and the work function (ϕ) [5,6]. For small or negative excess energies, the electrons are emitted from the tail of the Fermi-Dirac distribution and the MTE approaches the thermal limit $k_B T$ where k_B is the Boltzmann constant and T is the temperature of the electron distribution in the lattice [6,7]. At room temperature, the thermal limit is 25 meV, a result that has been experimentally verified from several systems like thin Sb films [8], Cu(100) [9], and graphene coated Cu(110) [10]. For small laser fluences, the electron distribution is essentially in equilibrium with the lattice and therefore the temperature of the electron distribution is equivalent to the temperature of the photocathode. Hence, the thermal limit can be reduced below 25 meV by cooling the photocathode to cryogenic temperatures. By cryogenically cooling the photocathode below liquid nitrogen temperatures (77 K), sub-10 meV MTEs have been measured from well-ordered single crystalline surfaces of Cu and graphene coated Cu when operating near zero excess energy [9,10]. In order to achieve these low MTEs, it is necessary that the photocathode is a well-ordered single crystal, as such surfaces minimize the MTE-degrading surface nonuniformities of physical and chemical roughness [11–13]. While these low MTEs represent a significant improvement on the 100–500 meV MTEs typically found in photoinjectors today, they come at the expense of an extremely low quantum efficiency or QE. For example, the QE of Cu in the near-zero-excess-energy regime is 10^{-7} at room temperature [14] and as low as 10^{-9} at liquid nitrogen temperatures [10]. In order to extract the large current densities necessary for XFELs and UED, a high laser fluence $> 10 \text{ mJ/cm}^2$ is required at room temperature for such photocathodes. However, at these high laser fluences, the nonlinear photoemission effects of multiphoton emission and electron heating begin to dominate the photoemission process and limit the minimum achievable MTE [15,16].

When considering photon energies close to the work function, two regimes related to the multiphoton emission phenomenon exist. The first is at negative excess energies where the energy of the photon is less than the work function and therefore an electron typically requires at least two photons to overcome the photoemission threshold. At negative excess energies near the photoemission threshold, it is still possible for single-photon emission to occur from the tail of the Fermi-Dirac distribution. However, this process represents only a small fraction of the total electron emission and most electrons are emitted via the

multiphoton process. The second regime occurs at positive, but small, excess energies under a large laser fluence. In this regime, at laser fluences higher than 10^{-3} mJ/cm^2 , linear photoemission is the dominant process. However, a small amount of multiphoton emission also occurs. Despite being only a small fraction of the total number of emitted electrons, the electrons emitted via the multiphoton emission process dominate the MTE due to their large emission energies [15]. It is this second regime that is relevant to photoinjectors as there is a tradeoff between extracting large current densities and achieving a small MTE.

Electron heating occurs when high laser fluences around 10 mJ/cm^2 are delivered to a sample by ps or sub-ps pulses and heat the electrons to several thousand Kelvin. At sub-ps timescales, the electron distribution is essentially thermally isolated from the lattice due to small electron-phonon coupling. The difference in heat capacities between the electron distribution and lattice leads to a heating effect of the electrons. The electron distribution and the lattice then reach an equilibrium on ps-timescales due to electron-phonon scattering [17,18]. A recent theoretical investigation looked at the impact that electron heating has on the MTE and showed that at high laser fluences and small excess energies, the minimum achievable MTE is limited by electron heating [16]. It was also shown that partial mitigation of electron heating can be achieved by irradiating the photocathode with pulse lengths on the order of 10 ps.

While the nonlinear processes of multiphoton emission and electron heating have been the focus of their own individual theoretical investigations [15,16], their relative strengths are not well understood. Experimentally, nonlinear effects have been briefly investigated, although many of these investigations were performed under certain experimental conditions that did not allow for a thorough characterization of the nonlinear effects. One such experiment measured multiphoton photoemission from polycrystalline copper [19]. However, these measurements only investigated multiphoton emission at negative excess energies and did not investigate the nonlinear effects above the threshold that emerge at high laser fluences. Another experiment measured the emittance of two-photon photoemission from polycrystalline copper in a UED beamline using the waist scan technique [20]. In this work, measurements were taken at a single positive excess energy and across a large range of laser fluences. By varying the laser fluence, they observed a transition from single- to two-photon photoemission with increasing fluence. However, these higher laser fluences led to large extracted charge densities causing space charge effects. It was not possible to clearly distinguish what portion of the emittance growth was due to two-photon emission or due to space charge effects. Recently, effects of MTE from Cu cathodes excited using a 130-fs tunable wavelength laser were measured at near-threshold negative excess energies using the time-of-flight technique [21]. All the above measurements were

performed for short 100 fs scale laser pulses. Photoinjectors often use longer 10 ps scale laser pulses followed by bunch compression to mitigate the effects of space charge. Theoretically, longer pulse lengths are expected to reduce the probability of nonlinear emission and mitigate its effects on MTE. However, this regime has never been studied experimentally with regard to its effects on MTE.

In this paper, we experimentally investigate the contribution that nonlinear photoemission effects have on the MTE of a graphene coated Cu(110) single crystal over a wide range of laser fluences, excess energies, and laser pulse lengths. We use these data to extrapolate the results to realistic photoinjector fluence and charge density conditions for a range of laser pulse lengths from 130 fs to 10 ps. In Sec. II, we describe the experimental setup. In Sec. III, we present detailed measurements that were performed. In particular, we present measurements of MTE at positive and negative excess energies, at a variety of laser fluences, and at laser pulse lengths of 130, 1, and 10 ps to investigate the impact that these various parameters have on nonlinear photoemission. In addition, we measured the total energy and transverse momentum distributions to provide deeper insights into the photoemission process. Finally, in Sec. IV, we discuss an extrapolation technique that allows us to obtain the effects of nonlinear photoemission on MTE at charge densities relevant to photoinjectors. Our results show that nonlinear effects play a dominant role when trying to reduce the MTE by lowering the excess energy and that high QE photocathodes will be essential for mitigating these effects.

II. EXPERIMENTAL SETUP

For this work, a graphene layer was grown on a commercially purchased Cu(110) single crystal according to the recipe found in Ref. [10]. After growth, the cathode was transported in air into our UHV analysis chamber for surface and photoemission measurements. The UHV chamber has a base pressure of 2×10^{-10} torr. The sample was annealed to 345°C for 2 h to produce a well-ordered atomically clean surface of graphene coated Cu(110) as evidenced by low-energy-electron-diffraction [10].

The energy and transverse momentum distributions were measured using a time-of-flight based analyzer [22]. It consists of the photocathode and a delay-line detector arranged in a parallel plate configuration and separated by ~ 4 cm. A short laser pulse is focused down to a sub-50 μm spot size on the photocathode and the emitted electrons are accelerated toward the detector by a voltage of 72 V. The relatively large accelerating voltage of 72 V compared to the 4 V used for previous high resolution studies is essential to measure the large MTE contributions from multiphoton effects. However, this causes the energy resolution of the measurement to be worse than 100 meV [22]. The delay-line detector measures the time of flight of the electrons as well as their x and y positions on

the detector. From that, the transverse and longitudinal energies and momenta can be calculated. The delay-line detector can detect at most one electron per pulse, and so neutral density filters are used to reduce the incident laser power and ensure that we are operating within that regime. While this step is necessary for the correct operation of the delay-line detector, it also ensures that our measurements are free of any space charge effects.

Tunable wavelength UV light was generated using an optical parametric amplifier (LightConversion ORPHEUS) pumped by a 130-fs pulse width 500-kHz repetition rate laser (LightConversion PHAROS). The sample was irradiated with photon energies ranging from 4.35 to 3.70 eV. The laser is p polarized and is incident at an angle of 50° with respect to the normal, and it was focused down to a spot size between 30 and 40 μm . While the spot size changed slightly, the location of the electron emission on the sample remained the same. The spot size was measured using a beam profiler used as a virtual cathode for all pulse lengths and photon energies. This spot size along with the pulse energy was used to calculate the fluence. All spot sizes quoted in this paper are measured as full width half max.

MTE measurements were performed at 130 fs, which is the natural pulse width of the laser, as well as at the stretched pulse lengths of 1 and 10 ps. The pulse was stretched from 130 fs to 1 ps and 10 ps using a pair of transmission diffraction gratings as shown in the schematic in Fig. 1. The diffraction gratings are made from fused silica and have an efficiency between 70% and 90% in our operating photon energy range [23]. This gives the pulse stretcher an overall efficiency of 15% to 39% in our photon energy range. From the schematic in Fig. 1, it can be seen that the laser is diverted from its original path and sent to the pulse stretcher where it passes through the first diffraction grating whose position is fixed. After it passes through the first diffraction grating, it is directed toward the second grating which is mounted to a 50-cm linear translator stage. The linear translator sets the distance between

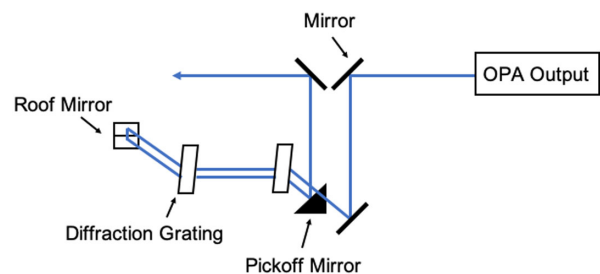


FIG. 1. The schematic of an in-house pulse stretcher that was built using a pair of transmission diffraction gratings. The schematic shows the pulse stretcher in relation to the optical parametric amplifier (OPA) output. By fixing one diffraction grating and moving the other, we can set the correct distance according to Eq. (4) and stretch the pulse to lengths ranging from 1 and 10 ps for photon energies between 3.70 and 4.77 eV.

the two diffraction gratings so that the desired pulse length can be achieved for a wide range of photon energies according to

$$L = \tau \cdot \frac{c[1 - (10^{-6}d\lambda - \sin\alpha)^2]^{3/2}}{2(10^{-6}d)^2\lambda\Delta\lambda}, \quad (4)$$

where L is the distance between diffraction gratings, τ is the pulse length of the stretched pulse, d is the line density, λ is the center wavelength of the laser, $\Delta\lambda$ is the bandwidth, α is the angle of incidence, and c is the speed of light [24]. After passing through the second diffraction grating, the beam hits a roof mirror that sends the beam back through both diffraction gratings at a slightly lower height. At this lower height, the beam hits the pickoff mirror, exits the pulse stretcher, and continues on its original path. The pulse duration was measured with a commercial autocorrelator [25] and the measured pulse length matched the expected pulse length calculated from Eq. (4).

III. EXPERIMENTAL RESULTS

The data were collected with photon energies ranging from 3.70 to 4.35 eV for 130 fs, 1 ps, and 10 ps pulse lengths. The QE and MTE measurements in the linear regime show the experimental work function of this photocathode to be 3.88 eV. With this work function, the photon energy range of 3.70–4.35 eV corresponds to -0.18 to 0.47 eV of excess energy. In this section, we present the MTE, QE, and energy distribution measurements at various photon energies and fluences for the three pulse lengths.

A. Mean transverse energy

Figure 2 shows MTE measurements taken between -0.18 eV excess energy and 0.47 eV excess energy for a 130-fs pulse length at a small enough fluence to keep the emission above the threshold fully linear. From this plot, we see that the minimum MTE occurs at zero excess energy which corresponds to the photoemission threshold of 3.88 eV. For excess energies between 0.2 and 0.476 eV, the MTE is approximately equal to one third of the excess energy as predicted by Eq. (3). As the positive excess energy approaches 0 eV, the MTE begins to deviate from Eq. (3) as it gets limited by the thermal limit to 25 meV. Below the photoemission threshold, the MTE increases dramatically as the nonlinear photoemission effects begin to dominate the MTE.

In order to investigate the impact that a changing laser fluence has on nonlinear photoemission effects, detailed measurements were performed right below the photoemission threshold for various laser fluences. At -0.06 eV excess energy, we can observe a transition between photoemission dominated by single-photon emission from

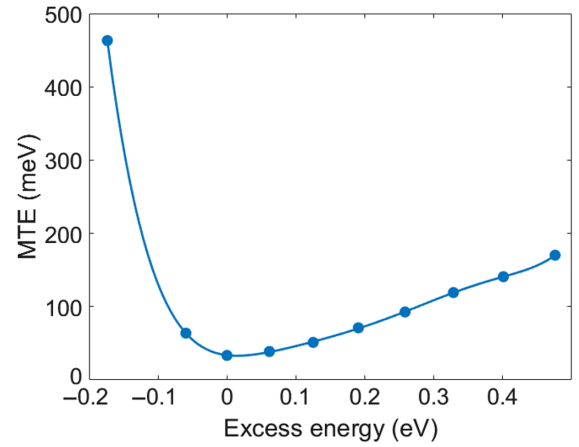


FIG. 2. Measured MTE as a function of excess energy for a 130-fs pulse length. The line joining the points is a guide for the eye. The laser fluence was kept small enough to ensure linear photoemission at 0 and positive excess energies. At large excess energies, the emission process is dominated by single-photon emission and the MTE is roughly equal to $E_{\text{excess}}/3$. At negative excess energies, the MTE increases significantly due to nonlinear photoemission effects. The error in the measurement was estimated to be 10%.

the tail of the Fermi-Dirac distribution to photoemission dominated by nonlinear effects. Figure 3 shows our measured data for the three pulse lengths at laser fluences between 10^{-4} mJ/cm² and 10^{-1} mJ/cm². For the 130-fs pulse length, we see that the MTE begins to increase at 10^{-4} mJ/cm² due to nonlinear effects, and that it increases by an order of magnitude at 10^{-2} mJ/cm² laser fluences. For the 1-ps data, the nonlinear effects begin to impact the

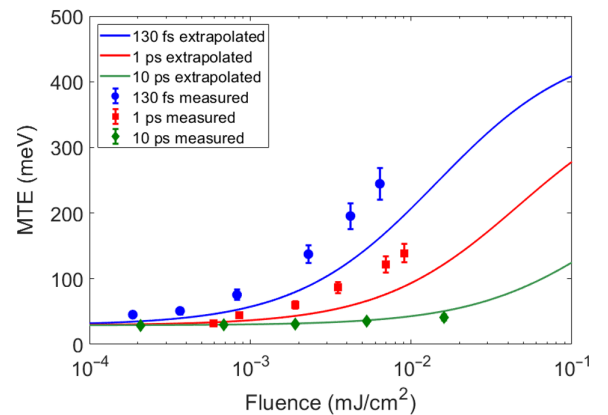


FIG. 3. Measured data points at -0.06 eV excess energy for 130 fs, 1 ps, and 10 ps pulse lengths as a function of laser fluence. At this excess energy, a significant increase in MTE is observed for the shorter pulse lengths due to nonlinear effects as the laser fluence increases. At the longer 10 ps pulse length, the increase in MTE is only a few meV for the highest laser fluence. The solid lines are obtained from the extrapolation technique described in Sec. IV. From this plot, we see that our extrapolation technique provides a lower limit on the MTE.

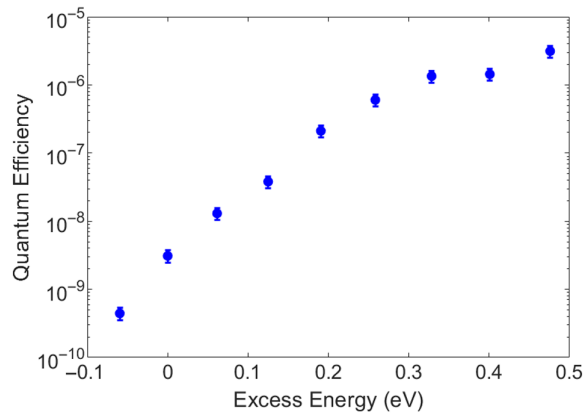


FIG. 4. Linear quantum efficiency as a function of excess energy for 130 fs. The current was measured from electron counts on the detector and therefore represents only a fraction of the actual current emitted. Hence the measured QE is some unknown factor on the order of unity lower than the actual QE.

MTE at 10^{-3} mJ/cm², and at 10^{-2} mJ/cm², the MTE is roughly a factor of 2 smaller than the 130-fs data. At 10-ps pulse lengths, the MTE only begins increasing slightly at 10^{-2} mJ/cm². As the delay-line detector cannot measure more than one electron per shot, we are unable to perform any direct measurements beyond this laser fluence.

B. Quantum efficiency

Figure 4 shows the measured QE that corresponds to the data points from Fig. 2. For this experiment, the QE is determined by treating each count measured by the detector as one electron. The detector efficiency may be less than one and hence this is only a lower estimate of the QE. From previous calibrations, we expect the detector efficiency to be a large fraction and hence the QE measurement is still accurate within the order of magnitude. From Fig. 4, we see that the QE is 10^{-9} at zero excess energy. This QE is very low compared to other metal photocathodes like bare polycrystalline copper which often exhibit a QE of 10^{-7} at zero excess energies [14]. All values presented in Fig. 4 are measured keeping the fluence small enough to be in the linear range.

C. Total energy distribution

Figure 5 shows the normalized total energy distribution for the three different pulse lengths at a photon energy of 3.82 eV (excess energy of -0.06 eV). These total energy curves correspond to the largest fluence measurements from Fig. 3 for each pulse length. This corresponds to a fluence of 6.4×10^{-3} mJ/cm² for the 130-fs curve, 9.1×10^{-3} mJ/cm² for the 1-ps curve, and 1.6×10^{-2} mJ/cm² for the 10-ps curve. The initial drop from 0 to ~ 100 meV corresponds to single-photon emission from the Fermi tail. As expected, this initial drop is largest for the 10-ps data which indicates that the

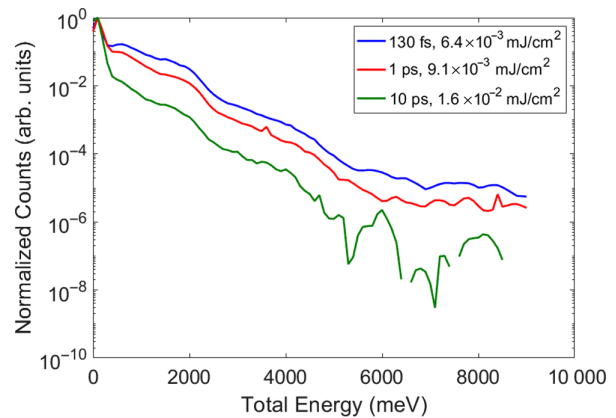


FIG. 5. Total energy distribution at 325 nm (-0.06 eV excess energy) for 130 fs, 1 ps, and 10 ps. We see that multiphoton emission is significantly reduced and the number of electrons emitted from a single photon is increased for the 10-ps data. This shows that multiphoton can be significantly mitigated by operating at 10 ps pulse lengths.

fraction of electrons emitted via single-photon emission is largest for 10 ps. From 100 to 4000 meV, we see two-photon emission for all three pulse lengths. Around 2000 meV, we see a similar feature in all three curves. Looking at the density of states of Cu, there is an increased number of electrons at -2000 meV corresponding to the d band [26]. Hence, it is possible that this feature at 2000 meV can be attributed to the d band. Beyond 4000 meV, we see the presence of three-photon emission for the 130-fs and 1-ps data while the 10 ps shows mostly noise. Comparing the three curves we see that the drop between 130 fs and 1 ps is significantly smaller than the drop between 1 and 10 ps suggesting a significant change in the photoemission process at the 10-ps time scales.

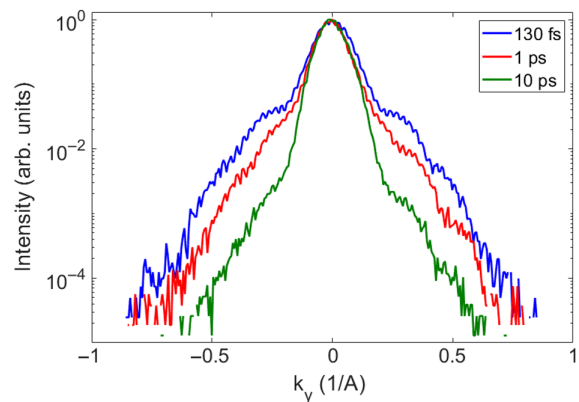


FIG. 6. The $k_x = 0$ slice of the energy integrated transverse momentum distribution on a log scale for 130 fs, 1 ps, and 10 ps under the same photoemission conditions as shown in Fig. 5. The small wiggles are an artifact of a mesh grid placed at the entrance of the detector.

D. Transverse momentum distribution

Figure 6 shows the $k_x = 0$ slice of the energy integrated transverse momentum distribution on a log scale for the same photoemission conditions shown in Fig. 5. All three curves fall sharply till 0.25 1/\AA , beyond which the emission is dominated by the two-photon process. The sharp drops beyond 0.25 1/\AA correspond to the emission of d-band electrons and the three-photon process, respectively, just like in Fig. 5.

IV. EXTRAPOLATION TO LARGER FLUENCES

While the data presented in the previous section gives a much needed starting point for the contribution of nonlinear photoemission on the MTE, it does not provide us measurements at laser fluences between 0.1 mJ/cm^2 and 4 mJ/cm^2 and excess energies in the range of $0\text{--}1 \text{ eV}$ which are typically used in photoinjectors. For the smallest laser spot size achievable in the energy analyzer, this range of fluence and excess energies leads to more than one electron being emitted per shot and hence cannot be measured by the delay-line detector. In order to estimate the MTE in the fluence and excess energy range typically used in photoinjectors, we have used the measurements presented in Sec. III and devised an extrapolation scheme based on the extended Fowler-Dubridge theory.

From the extended Fowler-Dubridge theory for nonlinear photoemission, the total photocurrent density can be expressed as a sum of the partial current densities for n -photon emission (J_n) according to the following relation:

$$J = \sum_{n=0}^{\infty} J_n = \sum_{n=0}^{\infty} \beta_n I^n, \quad (5)$$

where J is the total photocurrent density, β_n is the expansion coefficient, I is the intensity of the irradiating laser, and n is an integer corresponding to n -photon emission [27]. For our extrapolation, we have considered only single- and two-photon emission and represented the MTE as a sum of partial MTEs. With such an extrapolation, the MTE can be given as a function of the fluence F as

$$\text{MTE} = \frac{1}{N} \left(\frac{N_L \cdot \text{MTE}_L}{F_L/F} + \frac{N_{NL} \cdot \text{MTE}_{NL}}{(F_{NL}/F)^2} \right), \quad (6)$$

where $N_{L,NL}$ is the number of electron counts per second, $\text{MTE}_{L,NL}$ is the MTE, $F_{L,NL}$ is the laser fluence, and the subscripts L and NL represent the linear and nonlinear contributions, respectively. N is calculated according to

$$N = \frac{N_L}{F_L/F} + \frac{N_{NL}}{(F_{NL}/F)^2}. \quad (7)$$

Since the linear emission does not change significantly across the three pulse lengths, we have taken one dataset

TABLE I. A table showing the data used in the extrapolation technique. The dataset titled ‘‘Linear’’ is used in the extrapolation for all three pulse lengths as the linear contribution. While the nonlinear contributions are titled ‘‘130 fs,’’ ‘‘1 ps,’’ and ‘‘10 ps’’ for the respective pulse lengths. The linear data are at an excess energy of -0.06 eV while the nonlinear data are at an excess energy of -0.18 eV .

Data	MTE (meV)	N (counts/s)	F (mJ/cm^2)
Linear	29	850	1.9×10^{-4}
130 fs	463.12	6700	4.6×10^{-3}
1 ps	394.87	14 000	1.2×10^{-2}
10 ps	306.55	2000	7.3×10^{-3}

that was collected at 130 fs and used it as the linear contribution for all three pulse lengths. For the nonlinear contribution, we have taken measurements at -0.18 eV excess energy for each pulse length. The specific linear and nonlinear datasets used are shown in Table I.

This extrapolation technique assumes that the contribution of nonlinear effects to the MTE does not change significantly from -0.18 eV to other excess energies and does not change significantly at laser fluences larger than 10^{-2} mJ/cm^2 . Our technique also assumes only second order photoemission effects and ignores any high order effects as well as the effects of electron heating. Due to these assumptions, our extrapolation technique only provides a lower limit for the MTE.

A. Mean transverse energy and laser fluence

In order to check the accuracy of our extrapolation, we have compared it with our measured data as shown in Fig. 3 for excess energy of -0.06 eV . We can see that the extrapolation curves are in good agreement with the measured data for all the pulse lengths. In addition, we see that all extrapolated values are smaller than the measured data. This is expected because the extrapolation only gives a lower limit for the MTE.

Figure 7 shows the extrapolation over the 10^{-4} to 10^0 mJ/cm^2 fluence range. The curves are identical to those presented in Fig. 3, except at higher laser fluences. We see that nonlinear effects begin to contribute to the MTE at laser fluences as low as 10^{-4} mJ/cm^2 for 130-fs pulse lengths and at 10^{-2} mJ/cm^2 for 10-ps pulse lengths. This is as expected since the 2 orders of magnitude difference between pulse lengths is compensated by the 2 orders of magnitude difference in laser fluence. Finally, we see in Fig. 7 that at higher fluences, the curves begin to plateau. This is a limitation of the extrapolation technique and occurs because of not considering the effects of third order and higher photoemission. In reality, we do not expect these curves to plateau, but we expect them to continue increasing as the laser fluence increases.

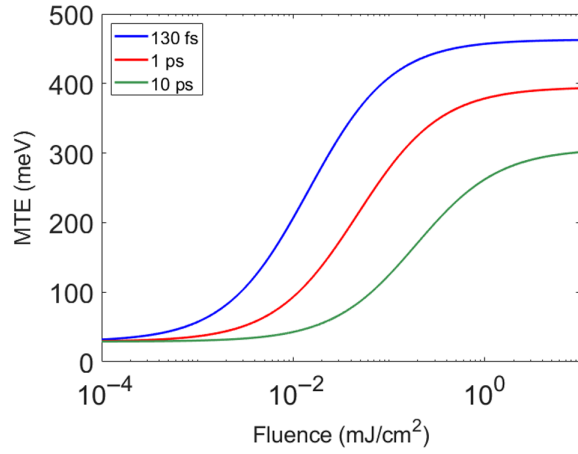


FIG. 7. MTE vs fluence curves for 130 fs, 1 ps, and 10 ps pulse lengths calculated from Eq. (6). Although the curves plateau at higher fluences, this is an artifact of not including beyond second order photoemission in the extrapolation technique. In practice, we would expect the curves to continue rising with fluence due to third and higher order photoemission effects. The curves are identical to those presented in Fig. 3, except at higher laser fluences.

B. Mean transverse energy and charge density

While Fig. 7 provides us with some insight into the fluence range where nonlinear effects begin to impact the MTE for a particular excess energy, we are more interested in the MTE we can expect at various charge densities that are relevant to photoinjectors. In particular, we want to identify the ideal operating excess energy that results in the minimum MTE for a given charge density per bunch. For that, we have calculated the charge density as a function of the fluence (F) and excess energy as

$$CD = \frac{Nq}{Af}, \quad (8)$$

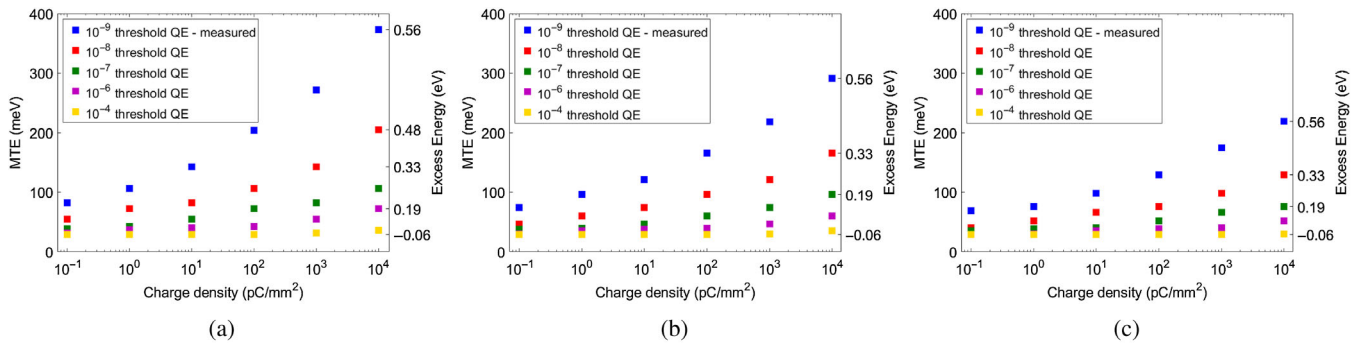


FIG. 8. Minimum contribution to the MTE from nonlinear effects as calculated from Eq. (8) for charge densities ranging from 10^{-1} and 10^4 pC/mm² for (a) 130 fs, (b) 1 ps, and (c) 10 ps pulse widths. The calculation was performed for the measured QE data as well as for higher QEs. It shows that a nearly full mitigation of nonlinear effects can be achieved by using photocathodes with QEs on the order of 10^{-4} at the threshold.

where N is the number of electrons calculated from Eq. (7), q is the charge of the electron, A is the emission spot area, and f is the repetition rate of our laser (500 kHz). In this case, we used the data from Fig. 2 for positive excess energies as the linear contribution to Eq. (6). Then we calculated the extracted charge density and MTE as a function of the fluence for various excess energies. By checking over all of the measured excess energies, we were able to identify the minimum MTE that we can expect for a given charge density and the excess energy where this minimum occurs.

Figure 8 shows the minimum MTEs at various charge densities for the three pulse lengths along with the excess energy at which this minimum occurs on the right y axis. Figure 8 also shows curves for this minimum MTE obtained by scaling the measured linear QE presented in Fig. 4 by various factors ranging from 10 to 10^5 . We plot this for charge density ranges that are often used in dc and rf photoinjectors.

From Fig. 8, we see that for all three pulse lengths, the 10^{-9} threshold QE dataset has an MTE that increases significantly with increasing charge density. We also see that for all charge densities the minimum MTE occurs at excess energies greater than 0.19 eV. This shows that for very low QE photocathodes, there needs to be a balance between contributions to the MTE from excess energy and from nonlinear effects in order to achieve the minimum MTE at these charge densities. Furthermore, we see that the minimum MTE is approximately a factor of 2 larger than the thermal limit at 10^{-1} pC/mm² for all three pulse lengths. This shows that cathodes with very low QE of 10^{-9} at threshold are not suitable for operating at these high charge densities and are really only suitable for applications that require a single-to-few electron per pulse.

For the 10^{-8} QE dataset, we see that at larger pulse lengths, the minimum MTE does occur right near the threshold for the smaller charge densities. However, at the large charge densities, we see a behavior similar to the

“measured QE” dataset with the minimum MTEs occurring at large excess energies. For charge densities in the 10^{-1} to 10^1 pC/mm², sub-100 meV MTEs can be achieved for all three pulse lengths. However, for higher charge densities, 10-ps pulse lengths must be used to achieve MTEs near 100 meV.

In general, the 10^{-9} QE, 10^{-8} QE, and 10^{-7} QE datasets correspond to QEs of metallic photocathodes. While the 10^{-9} QE and 10^{-8} QE datasets show a significant increase in MTE at high charge densities, at 10^{-7} QE, we see that it is possible to obtain sub-100 meVs even at these high charge densities for all three pulse lengths. However, at high charge densities, there still needs to be a balance between excess energy and nonlinear effects in order to achieve the smallest MTE.

Looking at the 10^{-4} QE data in all three plots, we see that for the entire range of charge densities, the minimum MTE is at or near the thermal limit of 25 meV and the excess energy is near zero. This indicates that there is no contribution to the MTE from nonlinear photoemission effects. Such high threshold QEs are possible from low-electron-affinity semiconductor cathodes. Therefore, to achieve MTEs near the thermal limit at charge densities as high as 10^4 pC/mm², it is essential to use high QE photocathodes like low-electron affinity semiconductors.

V. CONCLUSION

We have presented MTE measurements of nonlinear photoemission from a graphene coated Cu(110) photocathode above and below the photoemission threshold for pulse lengths of 130 fs, 1 ps, and 10 ps. Our results show that for a given laser fluence, the contribution to the MTE from nonlinear effects can be significantly reduced by using longer pulse lengths. At longer pulse lengths, the total energy and transverse momentum distributions show that the fraction of electrons emitted via single-photon emission is significantly larger in comparison to the shorter pulse lengths. In addition, we extrapolate our data to identify the minimum MTE that can be achieved at charge densities ranging from 10^{-1} to 10^4 pC/mm² for threshold QEs ranging from 10^{-9} to 10^{-4} . We show that when using lower QE photocathodes to obtain high charge densities, a balance between nonlinear effects and excess energy is necessary in order to achieve the minimum MTE. In addition, we show that for high charge densities, low MTEs near the thermal limit are not attainable for photocathodes with QEs less than 10^{-8} at threshold and hence such photocathodes are only practical for single-to-few electron per pulse applications. For photocathodes with QEs greater than 10^{-7} at threshold, we show that sub-100 meV MTEs can be attained at all relevant charge densities by tuning the excess energy appropriately. Finally, for photocathodes with QEs greater than 10^{-4} at threshold, we see no significant contribution to the MTE from

nonlinear effects for all pulse lengths and charge densities. Hence, it is essential that high QE photocathodes like low-electron affinity semiconductors are used for high charge density applications.

ACKNOWLEDGMENTS

This work was supported by the U.S. National Science Foundation under Grant No. PHY-1549132, the Center for Bright Beams, the Department of Energy under Grant No. DE-SC0021092, and by the U.S. Department of Energy (DOE) Office of Science under the U.S.-Japan Science and Technology Cooperation Program in High Energy Physics and the Japan Society for the Promotion of Science (JSPS) Grant-in-Aid for Scientific Research on Innovative Areas “Science of 2.5 Dimensional Materials: Paradigm Shift of Materials Science Toward Future Social Innovation” (KAKENHI Grants No. JP21H05232 and No. JP21H05233). The authors would like to thank Dr. Adam Bartnik and Professor Jared Maxson from Cornell University for their assistance in designing the pulse stretcher.

-
- [1] M. Ferrario, Overview of FEL injectors, in *Proceedings of the 10th European Particle Accelerator Conference, Edinburgh, Scotland, 2006* (EPS-AG, Edinburgh, Scotland, 2006).
 - [2] J. B. Rosenzweig *et al.*, An ultra-compact x-ray free electron laser, *New J. Phys.* **22**, 093067 (2020).
 - [3] P. Musumeci, J. T. Moody, C. Scoby, M. S. Gutierrez, H. A. Bender, and N. S. Wilcox, High quality single shot diffraction patterns using ultrashort megaelectron volt electron beams from a radio frequency photoinjector, *Rev. Sci. Instrum.* **81**, 013306 (2010).
 - [4] I. V. Bazarov, B. M. Dunham, and C. K. Sinclair, Maximum Achievable Brightness from Photoinjectors, *Phys. Rev. Lett.* **102**, 104801 (2009).
 - [5] D. H. Dowell and J. Schmerge, Quantum efficiency and thermal emittance of metal photocathodes, *Phys. Rev. ST Accel. Beams* **12**, 074201 (2009).
 - [6] P. Saha, O. Chubenko, J. Kevin Nangoi, T. Arias, E. Montgomery, S. Poddar, H. A. Padmore, and S. Karkare, Theory of photoemission from cathodes with disordered surfaces, *J. Appl. Phys.* **133**, 053102 (2023).
 - [7] T. Vecchione, D. Dowell, W. Wan, J. Feng, and H. A. Padmore, Quantum efficiency and transverse momentum from metals, in *Proceedings of FEL2013, New York, NY, USA* (Joint Accelerator Conferences Website (JACoW), Geneva, Switzerland, 2013), pp. 424–426.
 - [8] J. Feng, S. Karkare, J. Nasiatka, S. Schubert, J. Smedley, and H. A. Padmore, Near atomically smooth alkali antimonide photocathode thin films, *J. Appl. Phys.* **121**, 044904 (2017).
 - [9] S. Karkare, G. Adhikari, W. A. Schroeder, J. K. Nangoi, T. Arias, J. M. Maxson, and H. A. Padmore, Ultracold Electrons via Near-Threshold Photoemission from Single-Crystal Cu(100), *Phys. Rev. Lett.* **125**, 054801 (2020).

- [10] C. J. Knill, H. Yamaguchi, K. Kawahara, G. Wang, E. Batista, P. Yang, H. Ago, N. Moody, and S. Karkare, Near-threshold photoemission from graphene-coated Cu(110), *Phys. Rev. Appl.* **19**, 014015 (2023).
- [11] S. Karkare, J. Feng, X. Chen, W. Wan, F. J. Palomares, T.-C. Chiang, and H. A. Padmore, Reduction of Intrinsic Electron Emittance from Photocathodes Using Ordered Crystalline Surfaces, *Phys. Rev. Lett.* **118**, 164802 (2017).
- [12] S. Karkare and I. Bazarov, Effects of surface nonuniformities on the mean transverse energy from photocathodes, *Phys. Rev. Appl.* **4**, 024015 (2015).
- [13] G. Gevorkyan, S. Karkare, S. Emamian, I. V. Bazarov, and H. A. Padmore, Effects of physical and chemical surface roughness on the brightness of electron beams from photocathodes, *Phys. Rev. Accel. Beams* **21**, 093401 (2018).
- [14] D. H. Dowell, F. K. King, R. E. Kirby, J. F. Schmerge, and J. M. Smedley, In situ cleaning of metal cathodes using a hydrogen ion beam, *Phys. Rev. ST Accel. Beams* **9**, 063502 (2006).
- [15] J. K. Bae, I. Bazarov, P. Musumeci, S. Karkare, H. A. Padmore, and J. Maxson, Brightness of femtosecond nonequilibrium photoemission in metallic photocathodes at wavelengths near the photoemission threshold, *J. Appl. Phys.* **124**, 244903 (2018).
- [16] J. M. Maxson, P. Musumeci, L. Cultrera, S. Karkare, and H. A. Padmore, Ultrafast laser pulse heating of metallic photocathodes and its contribution to intrinsic emittance, *Nucl. Instrum. Methods Phys. Res., Sect. A* **865**, 99 (2017).
- [17] S. I. Anisimov, B. L. Kapeliovich, and T. L. Perel'Man, Electron emission from metal surfaces exposed to ultrashort laser pulses, *Zh. Eksp. Teor. Fiz.* **66**, 776 (1974).
- [18] H. L. Elsayad-Ali, T. B. Norris, M. A. Pessot, and G. A. Mourou, Time-Resolved Observation of Electron-Phonon Relaxation in Copper, *Phys. Rev. Lett.* **58**, 1212 (1987).
- [19] C. An, R. Zhu, J. Xu, Y. Liu, X. Hu, J. Zhang, and D. Yu, Increase of intrinsic emittance induced by multiphoton photoemission from copper cathodes illuminated by femtosecond laser pulses, *AIP Adv.* **8**, 055225 (2018).
- [20] P. L. E. M. Pasmans, D. C. van Vugt, J. P. van Lieshout, G. J. H. Brussaard, and O. J. Luiten, Extreme regimes of femtosecond photoemission from a copper cathode in a DC electron gun, *Phys. Rev. Accel. Beams* **19**, 103403 (2016).
- [21] C. J. Knill, H. A. Padmore, and S. S. Karkare, Near-threshold nonlinear photoemission from Cu(100), in *Proceedings of the 12th International Particle Accelerator Conference, IPAC2021, Campinas, SP, Brazil* (JACoW, Geneva, Switzerland, 2021), WEPAB099.
- [22] S. Karkare, J. Feng, J. Maxson, and H. A. Padmore, Development of a 3-D energy-momentum analyzer for MeV-scale energy electrons, *Rev. Sci. Instrum.* **90**, 053902 (2019).
- [23] Ibsen (2022), <https://ibsen.com/product/uv-2847-916/>.
- [24] Z. Zhong, W. Gong, H. Jiang, H. Gu, X. Chen, and S. Liu, Investigation of spatial chirp induced by misalignments in a parallel grating pair pulse stretcher, *Appl. Sci.* **10**, 1584 (2020).
- [25] pulseCheck, <https://www.ape-berlin.de/en/autocorrelator/pulsecheck/>.
- [26] O. Bunau and Y. Joly, Self-consistent aspects of x-ray absorption calculations, *J. Phys. Condens. Matter* **21**, 345501 (2009).
- [27] G. Ferrini, F. Banfi, C. Giannetti, and F. Parmigiani, Non-linear electron photoemission from metals with ultrashort pulses, *Nucl. Instrum. Methods Phys. Res., Sect. A* **601**, 123 (2009).